Chinese Chemical Letters 35 (2024) 108567

Contents lists available at ScienceDirect

Chinese Chemical Letters

journal homepage: www.elsevier.com/locate/cclet

A review on g-C_3N_4 decorated with silver for photocatalytic energy conversion

Ziyu Pan, Wufan Ding, Hanchun Chen, Haodong Ji*

Eco-environment and Resource Efficiency Research Laboratory, School of Environment and Energy, Peking University Shenzhen Graduate School, Shenzhen 518055, China

ARTICLE INFO

Article history:
Received 8 January 2023
Revised 13 April 2023
Accepted 10 May 2023
Available online 12 May 2023

Keywords:
g-C_3N_4
Silver-modified g-C_3N_4
Photocatalytic energy conversion
H_2 evolution
Pollutant degradation
CO_2 reduction

ABSTRACT

Artificial photocatalytic energy conversion is considered as the most potential strategy for solving the increasingly serious energy crisis and environmental pollution problems by directly capturing solar energy. Therefore, high efficiency photocatalyst has drawn significant research attention in recent years. Due to the excellent electronic, optical, structural, and physicochemical performances, silver-based g-C_3N_4 have become promising photocatalysts. This review emphasizes the recent progresses and challenges on g-C_3N_4 decorated with silver for photocatalytic energy conversion. The extensive use of g-C_3N_4 decorated with silver in diverse photocatalytic reactions, including hydrogen evolution, pollutant degradation and carbon dioxide reduction, is also fully introduced. In addition, we propose the perspectives of g-C_3N_4 decorated with silver on photocatalytic applications. We hope that this review will shed some light on the photocatalytic energy conversion of g-C_3N_4 decorated with silver.

1. Introduction

Energy and good ecological environment are the cornerstone and indispensable element in today's the sustainable global development of human society [1,2]. With the rapid industrialization and globalization, energy shortage and environmental pollution have gradually escalated into hotspot issue [3–5]. However, depletable and unclean fossil fuels are still the main energy sources humans use nowadays [6]. Thus, exploring clean and inexhaustible energy is urgent to reverse the trend. The infinite and freely accessible solar energy is regarded as the most environmentally friendly and most promising new energy resource [7]. Artificial photocatalytic energy conversion supplies the promising manner for overcoming energy crisis, combating to climate change and remediating environment [6,8,9]. For instance, sustainable clean H_2 fuel, which was produced by photocatalytic water splitting [10–13], was considered as one of the most promising green energy sources due to generating water during the process of complete reaction between H_2 and O_2 [14]. The photocatalytic CO_2 reduction was widely recognized as a deployable and highly intriguing strategy to recycle the inert CO_2 into value-added substances such as CH_4 or CO [15]. The photocatalytic degradation of environmental contaminants could treat the wastewater economically and effectively [16,17]. Therefore, the development and improvement of photocatalysts that could effectively absorb photons from the sun need to be studied intensively and many encouraging achievements have been made after years of exploration.

Among various photocatalysts of zero-dimension, one dimension, two dimension and three-dimension, polymer semiconductor g-C_3N_4 has drawn immense attraction in recent years owing to its customizable structure, excellent visible-light response activity, superiorly photochemical and thermal stability, abundance of raw materials, facile synthetic strategy, low cost and toxicity [18,19]. As an n-type organic semiconductor, g-C_3N_4 possesses an optical band gap of 2.70 eV. Therefore, g-C_3N_4 can harvest visible light of the solar spectrum up to 460 nm [20–22]. Nevertheless, the further large-scale applications of g-C_3N_4 are restricted due to low surface area, severe charge recombination rate, low mobility of charge and inadequate visible light (wavelength range, 400–760 nm) absorption. To overcome such shortcomings, the composites with high photoactivity of g-C_3N_4 are designed and developed. For example, the lifetime of the charge carriers could be prolonged by the morphology control [23]. In addition, other ways, including metal or non-metal doping [24–27], constructing heterojunctions [28–30], surface modification [31,32], have also been employed to improve the photocatalytic properties of g-C_3N_4. Among them, it is universally accepted that semiconductor surfaces modification using noble metal nanoparticles such as silver (Ag) and gold could expand the light-harvesting range of visible-near-infrared light owing to the surface plasmon resonance effects [33–35]. Besides, the

* Corresponding author.
E-mail address: jihaodong@pku.edu.cn (H. Ji).

https://doi.org/10.1016/j.cclet.2023.108567
1001-8417/

noble metal nanoparticles could do duty for the electron trappers due to the low Fermi levels [36]. Compared to other noble metals, the Ag was regarded as the most economical raw materials that possessed the stronger surface plasmon resonance effect and higher sensitivity [37,38]. Thus, the Ag decoration has increasingly been considered as a promising method, which could facilitate separation/transfer of charge carriers and enhance the absorption of visible light so as to achieve the high photocatalytic energy conversion [39,40]. Currently, the synthetic methods of various Ag decorated g-C_3N_4 are generally calcination, chemical and photo-assisted reduction. Typically, Ag/g–C_3N_4 porous nanofibers was synthesized using supramolecular hydrogel of Ag-melamine as the precursor *via* calcination and presented highly efficient H_2 evolution [41]. The photo-assisted reduction using ultra-violet (UV) irradiation was applied to synthesize the Ag nanoparticles decorated g-C_3N_4 nanosheets [42]. Ag decorated P-doped g-C_3N_4 nanosheets, which visible-light photocatalytic activities were proved to significantly enhance by the experiments of water splitting and pollutant degradation, were constructed by silver mirror reaction and two-step calcination process [43]. Microfluidic reactors with the advantages of high heat and mass transfer, operational safety and enhanced scalability were also employed for Ag/g-C_3N_4 synthesis, achieving the higher catalytic activity for the photocatalytic water splitting [44]. Furthermore, single-atom Ag incorporated g-C_3N_4 catalyst was synthesized and presented excellent stability and higher photocatalytic activities for H_2 evolution than Ag or Pt nanoparticles decorated g-C_3N_4 [45] and so forth. As far as we know, although some excellent reviews have summarized the based-g-C_3N_4 applications such as H_2 evolution [46,47], pollutant degradation [48,49], and CO_2 reduction [50,51], the comprehensive review of g-C_3N_4 decorated with silver for photocatalytic energy conversion have not been covered.

In this review, we began with comprehensive and in-depth introductions for the basic performances and types of g-C_3N_4. Then, the g-C_3N_4 decorated with various silvers were introduced systematically, focusing on the comprehensive summary of g-C_3N_4 decorated with silver nanoparticles and single atom silver. It was worth noting that the composites of silver and g-C_3N_4 semiconductor possess unique advantage than other g-C_3N_4 composite photocatalyst, including enhancing visible light absorption, prolonging the lifetime of the charge carriers, excellent controllability and stability, higher photocatalytic efficiency and environmentally friendly. Therefore, the photocatalysts of g-C_3N_4 decorated with various silvers have become the promising candidates for photocatalytic energy conversion and environmental remediation. As shown in Fig. 1, their applications on H_2 evolution, pollutant degradation and CO_2 reduction were summarized. Finally, some pivotal challenges and perspectives for future development were further proposed.

2. Basic performances and types of g-C_3N_4

2.1. Basic performances of g-C_3N_4

Metal-free polymer semiconductor: The g-C_3N_4, consisting of triazine or tri-*s*-triazine units connected with planar amino groups in each layer and weak van der Waals force between layers, was just consist of carbon (C) and nitrogen (N) with the hybridization forms of sp^2, and some impurity hydrogen (H) [52], as shown in Fig. 2. The C/N stoichiometric ratio confirmed by theoretical calculation was 0.75. Nevertheless, the results of element analysis, which was different from the ideal scale model of 0.75, verified that average C/N atomic ratio was 0.72 and there were 2% H from uncondensed amino functions [53]. Besides, the photocatalytic applications of semiconductor were mainly determined by the valence band (VB) potential, conduction band (CB) potential

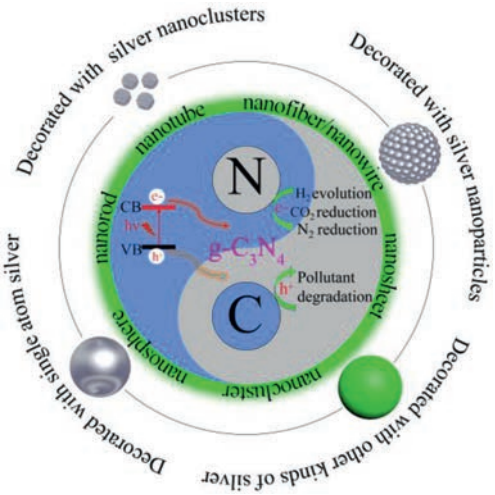

Fig. 1. Schematic illustration of the g-C_3N_4 decorated with various silvers for photocatalytic energy conversion.

and band gap energy (E_g). The VB and CB were severally due to the highest occupied molecular orbital (HOMO) and lowest unoccupied molecular orbital (LUMO). The E_g was the energy difference between the conduction band minimum (CBM) and valence band maximum (VBM) [3]. Therefore, the degree of light response and redox capability of semiconductor were controlled by the energy band structure (Fig. 1). The VB and CB of g-C_3N_4 were severally composed of nitrogen P_Z orbitals (HOMO) and carbon P_Z orbitals (LUMO) [44]. The E_g (2.70 eV) of g-C_3N_4 was the energy difference between VB (−1.1 eV) and CB (+1.6 eV) potential [54]. Thus, the g-C_3N_4 showed a response to visible light up to 460 nm [55,56]. In short, the simple composition of g-C_3N_4 endowed its unique characteristics such as nontoxic, biocompatible, easy preparation using abundant precursors, medium band gap, and made it become the promising candidate for the application system of visible light [57].

Stability: C_3N_4 processed five kinds of structures, including α-C_3N_4, β-C_3N_4, cubic C_3N_4, *quasi*-cubic C_3N_4 and graphite-like phase C_3N_4. Among them, the g-C_3N_4 was most stable due to the planar lamellae structure similar to graphene and had high thermal and chemical stability [58]. Thermal analysis showed that the heat resistance temperature was 600 °C in the air and complete decomposition temperature was up to 700 °C [53,59,60]. The chemical attack such as acid, alkali, and organic solvents except for potassium permanganate and molten alkali metal hydroxide was stable [61], which benefited from strong covalent C–N bonds in each layer and interlayer van der Waals forces [60]. Thus, the stable g-C_3N_4 was widely perceived as a promising inert material for various applications of high temperature reactions and surface science in multifarious solvents [62,63].

Optical performances: The optical property of g-C_3N_4 was critical for visible light photocatalytic applications, which could be characterized using photoluminescence (PL) [64], ultraviolet-visible diffuse reflection spectrum (UV–vis DRS) [16] and electrochemiluminescence (ECL) [65]. According to statistics, the band-gap initial UV–vis absorption peak of g-C_3N_4 was in the 420–450 nm wavelength range, which belonged to a characteristic absorption of organic semiconductor. According to a previous report, with the increase of condensation temperature, the absorption edge of UV–vis spectrum generated bathochromic shift, indicating the condensation temperatures could affect the band gap (Fig. 3A) [66]. In addition, doping of metallic and nonmetallic elements (Fe, Mn, Au, Ag, S, P, C, I, O, and B atoms and barbituric acid) also made the adsorption edge move towards longer wavelengths [53,67]. Coincidentally, condensation temperature also played a vital role in the PL. The PL

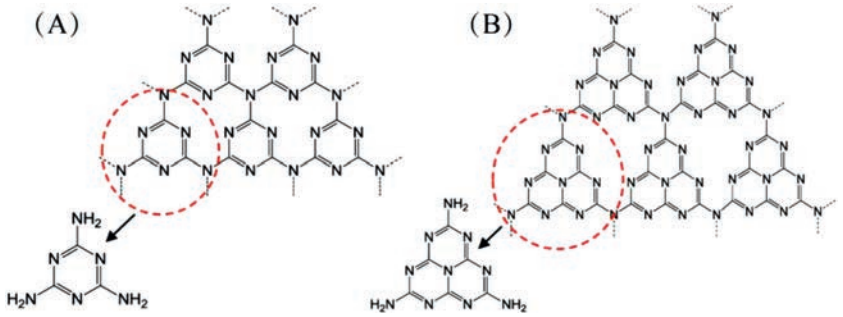

Fig. 2. (A) Triazine and (B) tri-*s*-triazine (heptazine) structures of g-C_3N_4. Reprinted with permission [73]. Copyright 2016, American Chemical Society.

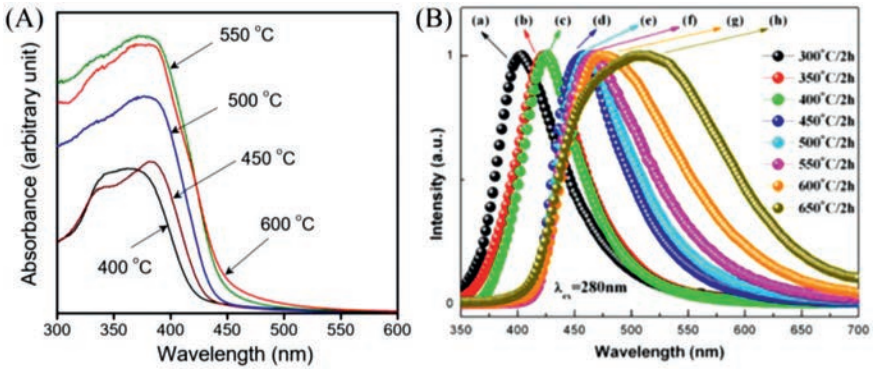

Fig. 3. (A) Ultraviolet-visible diffuse reflectance spectrum of g-C_3N_4 prepared at different temperature. Reprinted with permission [66]. Copyright 2009, Springer Nature. (B) Photoluminescence spectra of 2 h calcined g-C_3N_4 at different temperatures. Reprinted with permission [53]. Copyright 2022, Elsevier.

spectra of g-C_3N_4 were red shift when the condensation temperature increased (Fig. 3B). Furthermore, because of the transition of the *s*-triazine ring, the g-C_3N_4 dissolved in solvents emitted blue PL approximate 450 nm under UV light irradiation [68]. The ECL of g-C_3N_4 opened up a potential route for sensitive detection system, in which g-C_3N_4 acted as a donor of energy transfer [69]. In a word, the UV–vis DRS, PL and ECL properties of g-C_3N_4 were very important for applications in various fields such as catalysis, energy storage technologies, sensing, light-emitting devices, and biological imaging [70].

Electrochemical and photoelectrochemical performances: The strong electron acceptance ability of nitrogen atom in the heptaphane ring was in connection with the electrocatalytic performance of g-C_3N_4 and could induce the electrochemical reactions [60]. However, the single g-C_3N_4 was inert to the electrocatalysis common reactions of O_2 and H_2 evolution reaction [71]. There is no doubt that photoelectrochemical properties could endow g-C_3N_4 more excellent catalytic activity by the combination of optical and electrical performances, which opened the door for the study of photoelectrochemical performances of g-C_3N_4-based materials [72,73].

2.2. Types of g-C_3N_4

The types of g-C_3N_4 were still being extended due to the intense studies in the past few years. Synthetic routes, material compositions, condensation temperatures and shapes of g-C_3N_4 were pivotal for its properties and applications. The various types of g-C_3N_4 could be synthesized using various precursors, including melamine [74–76], urea [77,78], thiourea [79,80], dicyandiamide [81,82], cyanamide [83,84], and guanidinium chloride [85,86], and various suitable synthetic routes such as thermal condensation [87] and supramolecular pre-assembly [88]. In order to give a clearer picture of the morphologies, we classified herein in terms of different shapes, as shown in Fig. 4. The following was an introduction to the common and different shapes of g-C_3N_4 according to the timeline.

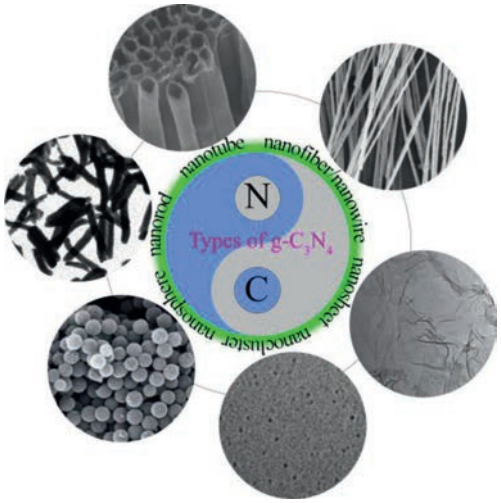

Fig. 4. Various morphologies of the g-C_3N_4. The nanocluster. Reprinted with permission [89]. Copyright 2014, Royal Society of Chemistry. The nanosphere. Reprinted with permission [97]. Copyright 2019, Royal Society of Chemistry. The nanorod. Reprinted with permission [99]. Copyright 2012, Royal Society of Chemistry. The nanotube. Reprinted with permission [103]. Copyright 2009, American Chemical Society. The nanofiber. Reprinted with permission [107]. Copyright 2008, Wiley. The nanosheet. Reprinted with permission [113]. Copyright 2012, Wiley.

Nanocluster and nanosphere: The strong quantum confinement effects of g-C_3N_4 nanoclusters when the size was less than 10 nm made it display the bright fluorescence. Besides, the advantages of g-C_3N_4 nanoclusters also contained good stability, non-toxicity and biocompatibility. The synthetic routes of g-C_3N_4 nanoclusters mainly contained two methods of top-down and bottom-up.

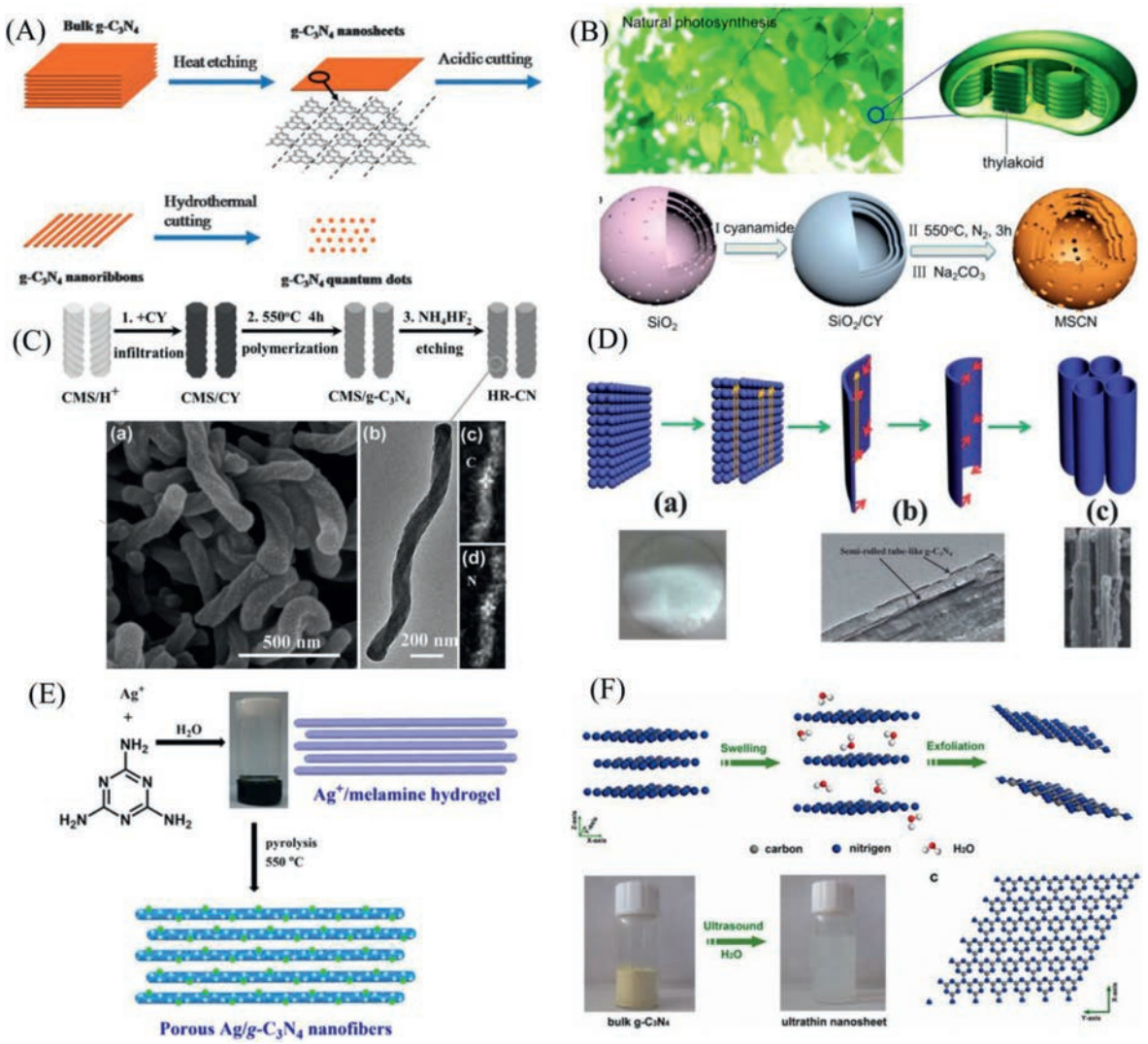

Fig. 5. (A) Schematic illustration of the controllable synthesis of g-C_3N_4 nanosheets, nanoribbons and quantum dots. Reprinted with permission [89]. Copyright 2014, Royal Society of Chemistry. (B) Overall synthetic procedure of multishell g-C_3N_4 nanocapsules. Reprinted with permission [84]. Copyright 2017, American Chemical Society. (C) Synthetic process for helical nanorod-like g-C_3N_4 and morphology characterization. Reprinted with permission [100]. Copyright 2014, John Wiley and Sons Ltd. (D) The proposed formation process of g-C_3N_4 nanotubes. Reprinted with permission [104]. Copyright 2014, Royal Society of Chemistry. (E) Preparation of porous nanofiber-like Ag/g-C_3N_4 from Ag-melamine supramolecular hydrogels. Reprinted with permission [41]. Copyright 2017, American Chemical Society. (F) Schematic illustration of liquid-exfoliation process from bulk g-C_3N_4 to ultrathin nanosheets, the photograph of bulk g-C_3N_4 and suspension of ultrathin g-C_3N_4 nanosheets. Reprinted with permission [115]. Copyright 2013, American Chemical Society.

The upconverted g-C_3N_4 nanoclusters were synthesized using the top-down method. Wang *et al.* prepare the g-C_3N_4 nanostructure by controlling the process of cutting three-dimensional bulk g-C_3N_4 into two-dimensional nanosheets, one-dimensional g-C_3N_4 nanoribbons and finally to zero-dimensional g-C_3N_4 nanostructures for the first time [89], as shown in Fig. 5A. In the same year, Xie *et al.* firstly prepared the g-C_3N_4 single-layered quantum dots using the top-down method which included three steps of acid treatment, hydrothermal treatment and ultrasonication [90]. Hu *et al.* also developed an extremely simple and green hydrothermal treatment of bulk g-C_3N_4 to form g-C_3N_4 dots for the first time [91]. The following year, the g-C_3N_4 quantum dots were prepared by bottom-up method. For example, Lin *et al.* developed a facile one-pot microwave-assisted solvothermal method to prepare the strong excitation-dependent photoluminescence g-C_3N_4 quantum dots [92]. Lu *et al.* prepared the oxygen and sulfur co-doped g-C_3N_4 quantum dots by thermal treatment of citric acid and thiourea, which had the strong blue photoluminescence [93]. Afterwards, the doping and metal modified methods were used to synthesize g-C_3N_4 quantum dots, which the emission wavelength was in the whole visible-light regime and exhibited excitation-dependent red emission peak by metal-enhanced effect [75,94]. The g-C_3N_4 nanospheres which the size was greater than 10 nm had been prepared using rapid microwave-hydrothermal method as early as in 2008 [95]. Interestingly enough, inspired by natural photosynthesis system, the spherical and multishell g-C_3N_4 nanocapsule was successfully synthesized by Shen *et al.*, which exhibited excellent visible-light harvesting and electron transfer properties [84], as illustrated in Fig. 5B. In recent years, the g-C_3N_4 microspheres and nitrogen-doped hollow carbon nanospheres were synthesized by facile thermal heating method and the classic Stöber approach [96,97], respectively.

Nanorod, nanotube, nanofiber/nanowire: The g-C_3N_4 nanorod, nanotube and nanofiber/nanowire belonged to the one-dimensional nanostructures and processed high surface area, smooth carrier transport and light harvesting. Thus, they were widely used in the field of photocatalysis. One's early years, the g-C_3N_4 nanorods and mesoporous g-C_3N_4 nanorods were success-

fully synthesized using chiral silica nanorods and SBA-15 nanorod as templates, respectively [98,99]. Interestingly enough, Zheng *et al.* reported a nanocasting approach to prepare twisted hexagonal rod-like C_3N_4 by using chiral silicon dioxides as templates [100], as illustrated in Fig. 5C.

As early as in 2004, the high-quality carbon nitride nanotubes, which inner diameters and wall thicknesses were severally in the range of 50–100 nm and 20–50 nm, were successfully synthesized by a simple benzene-thermal process and without using any catalyst or template for the first time [101]. Subsequently, the g-C_3N_4 nanobelts and nanotubes were produced by polycondensation of dicyandiamide and melamine at 290 °C and 4.5–5 MPa [102]. The polymerization reaction between ethylenediamine and carbon tetrachloride was used to produce carbon nitride nanotubes, in which the porous anodic aluminum oxide membranes played a templated role [103]. The nanotube-type g-C_3N_4, which showed blue fluorescence and excellent visible-light photocatalytic activity, was synthesized by facile and generally feasible method of directly heating melamine [104], as illustrated in Fig. 5D. The tapered hollow g-C_3N_4 composite nanotubes were fabricated *via* one-step thermal condensation of polyacrylonitrile, melamine and sulfur [105]. The tubular g-C_3N_4 isotype heterojunction, which could jointly manipulate the oriented transfer of electrons and holes so as to facilitate the visible-light photocatalysis, was produced by combining the molecular self-assembly and thermal polycondensation techniques [106].

Initially, the nitrogen-rich carbon nitride microfibers were large-scale synthesized by evaporating the as-synthesized graphitic carbon nitride precursor [107]. Subsequently, the g-C_3N_4 nanowires were synthesized by using diatom frustules as a substrate [108]. The following year, Tahir *et al.* also reported a facile, scale up, and efficient method to synthesize the g-C_3N_4 nanofibers, which could be used for energy storage and photodegradation of rhodamine B [109]. In recent years, the porous nanofiber-type g-C_3N_4 nanocomposites were fabricated by a new and facile supramolecular hydrogel self-template approach [41], as illustrated in Fig. 5E.

Nanosheet: The g-C_3N_4 nanosheets had received tremendous attention due to a graphite-like layered structure and weak van der Waals of interlamination and had been used widely in energy conversion applications [110–112]. Similar to aforementioned synthetic routes of g-C_3N_4 nanostructures, the g-C_3N_4 nanosheets mainly had two synthetic approaches, including the top-down and bottom-up approach. Niu *et al.* used the top-down chemical etching approach to produce the g-C_3N_4 nanosheets with larger surface area 306 m^2/g than the 50 m^2/g of bulk g-C_3N_4 [113]. The following year, Yang *et al.* [114] and Zhang *et al.* [115] demonstrated the synthesis of g-C_3N_4 nanosheets by liquid phase exfoliation routes, as illustrated in Fig. 5F. Subsequently, Ma *et al.* developed a new approach of sonication-exfoliation to fabricate proton-functionalized ultrathin g-C_3N_4 nanosheets for the first time [116]. Schwinghammer *et al.* synthesized crystalline carbon nitride nanosheets by one-step liquid exfoliation of bulk material poly(triazine imide) [117]. Recently, Chen *et al.* reported a barbituric acid-modified graphitic carbon nitride nanosheets with blue-green fluorescence, which were prepared by the copolymerization of dicyandiamide with barbituric acid and then the chemical oxidation process [118]. For the bottom-up approach, Yang *et al.* demonstrated the successful fabrication of graphene-based carbon nitride nanosheets using the nanocasting technology, which the graphene-based mesoporous silica nanosheets were employed as a template for the first time [119]. In the same year, Zhang *et al.* developed a new, facile, sulfur-mediated method to prepare the g-C_3N_4 polymers, which the big atomic size of sulfur could influence the conformation and the connectivity of the acquired g-C_3N_4 and hence provide a template tool for tuning the texture and electronic structure [120]. In addition, other methods have also been used to synthesize g-C_3N_4 nanosheets. For example, Cheng *et al.* obtained g-C_3N_4 nanosheets by pyrolyzing a melamine-KBH_4 mixture for the first time, which could be used as a fluorosensor for Cu^{2+} and possessed the chemiluminescence (ECL) behavior and so on [21].

3. The photocatalytic reactions of silver-modified g-C_3N_4

In recent years, considerable efforts had been done in the area of silver-modified g-C_3N_4 composite materials and a lot of achievements had been accomplished. For example, the silver nanoparticles, silver nanoclusters, single atom silver and other kinds of silver such as silver halides and silver phosphate were used to decorate the various g-C_3N_4 in order to effectively improve the photocatalytic activity of g-C_3N_4. There were mainly the following reasons. Firstly, the silver was relatively inexpensive compared with other noble metals such as Au and Pt. Then, the plasma resonance effect of metal Ag could facilitate the improvement of local electromagnetic fields and improve the electron conductivity, which could promptly generate the electron and hole carriers in photocatalysts. In addition, the Schottky junction between Ag and the g-C_3N_4 could restrain the recombination of electron and hole charge carriers [121–123]. In this focused section, the synthetic strategies of miscellaneous composite materials and the applications photocatalytic energy conversion of silver-decorated g-C_3N_4 were presented in detail. Furthermore, the reports on silver-decorated g-C_3N_4 photocatalysts were summarized in Table 1 following chronological order.

3.1. The g-C_3N_4 decorated with silver nanoparticles

In recent ten years, silver (Ag) nanoparticles decorated g-C_3N_4 had drawn broad interdisciplinary attention, which could be used for photocatalytic energy conversion such as photocatalytic pollutant degradation, photocatalytic hydrogen evolution, photocatalytic N_2 (highly stable) reduction [124], and sensing. As early as in 2011, Ge *et al.* synthesized the g-C_3N_4 photocatalysts loaded with noble metal Ag nanoparticles by facile heating method. The as-synthesized Ag/g-C_3N_4 composite with enhanced photocatalytic property was used for the decomposition of methyl orange and hydrogen evolution [125]. Yang *et al.* also prepared the Ag/g-C_3N_4 plasmonic photocatalysts *via* thermal polymerization and photodeposition method, which were used to effectively degrade the methyl orange and *p*-nitrophenol [126]. Whereafter, the organic pollutants, including methyl mercaptan [127], sulfamethoxazole [122], rhodamine B [128], and methylene blue [129], also were degraded under visible light by using the Ag/g-C_3N_4 composites as the photocatalyst. For the photocatalytic hydrogen evolution, Wang *et al.* had further proved that the promising photocatalyst of Ag/g-C_3N_4 exhibited highly promoted photoinduced electron-hole separation capability, so giving much better hydrogen evolution activity than the pristine g-C_3N_4 [41]. Recently, a wide variety of Ag/g-C_3N_4 photocatalysts, including the g-C_3N_4 nanotubes [130], bulk g-C_3N_4 [131], two-dimensional g-C_3N_4 nanosheets [78,132] decorated with silver nanoparticles, were designed and fabricated for photocatalytic hydrogen evolution under visible light, which all showed the enhanced charge separation/transfer owing to the introduction of silver nanoparticles. For instance, Fig. 6A showed the photocatalytic mechanism of hydrogen generation of Ag/g-C_3N_4. The electrons and holes formed, and then the electron injected into Ag nanoparticles sites. Schottky barrier between Ag and g-C_3N_4 could capture the photogenerated electrons and facilitate the separation rate of electron-hole pairs. Finally, the photoelectron reacted with the H_2O and generated hydrogen. Fig. 6B showed that the hydrogen generation rate increased dramatically with the increase of the loading content [132]. In addition, Yao *et al.* prepared the boron and noble metal Ag modified graphitic carbon

Table 1
Recent reports on g-C3N4-based photocatalysts.

Catalysts composition	Precursors	Photocatalyst applications	Ref.
Ag nanoparticles/g-C_3N_4	Melamine, $AgNO_3$	Decomposition of methyl orange and hydrogen evolution	[125]
Ag nanoparticles/g-C_3N_4	Urea, $AgNO_3$	Degradation of methyl orange and p-nitrophenol	[126]
Ag nanoparticles/g-C_3N_4	Melamine, $AgNO_3$	Disinfection	[123]
Ag nanoparticles/g-C_3N_4	Melamine, $AgNO_3$	Photocatalytic degradation of methyl mercaptan	[127]
Ag nanoparticles/g-C_3N_4	Melamine, $AgNO_3$	Photocatalytic hydrogen generation	[41]
Ag nanoparticles/g-C_3N_4	Melamine, $AgNO_3$	Ultrasensitive detection of heparin	[75]
Ag nanoparticles/g-C_3N_4	Urea, $AgNO_3$	Photocatalytic degradation of sulfamethoxazole	[122]
Ag nanoparticles/g-C_3N_4	Urea, $AgNO_3$	Photocatalytic degradation of rhodamine B	[128]
Ag nanoparticles/g-C_3N_4	Urea, $AgNO_3$	Photocatalytic water splitting for hydrogen (H_2) generation	[130]
Ag nanoparticles/g-C_3N_4	Dicyandiamide, $AgNO_3$	Photocatalytic nitrogen fixation	[133]
Ag nanoparticles/g-C_3N_4	Melamine, $AgNO_3$	Determination of organophosphorus pesticides	[134]
Ag nanoparticles/g-C_3N_4	Melamine, $AgNO_3$	Photocatalytic degradation of methylene blue and determination of Hg^{2+}	[135]
Ag nanoparticles/g-C_3N_4	Melamine, $AgNO_3$	Photocatalytic hydrogen production	[131]
Ag nanoparticles/g-C_3N_4	Urea, $AgNO_3$	Triboelectric nanogenerator	[42]
Ag nanoparticles/g-C_3N_4	Urea, $AgNO_3$	Photocatalytic hydrogen evolution	[78]
Ag nanoparticles/g-C_3N_4	Melamine, $AgNO_3$	Photocatalytic water splitting	[132]
Silver silicates dots/g-C_3N_4	Urea, $AgNO_3$	Degradation of rhodamine B and tetracycline	[55]
Ag@g-C_3N_4	Urea, $AgNO_3$	Photodegradation of methylene blue and rhodamine B dyes	[129]
Ag nanoclusters/g-C_3N_4	Urea, $AgNO_3$	Photodegradation of rhodamine B	[137]
Ag/AgO/g-C_3N_4	Melamine, $AgNO_3$	Degradation of acid violet-7 dye	[96]
Ag/g-C_3N_4	Dicyandiamide, $AgNO_3$	Photocatalytic ozonation of acetaminophen	[138]
Silver quantum dots/g-C_3N_4	Melamine, $AgNO_3$	Photocatalytic hydrogen evolution, degradation of rhodamine B	[136]
Ag/g-C_3N_4	Melamine, $AgNO_3$	Photocatalytic hydrogen evolution, degradation of rhodamine B	[43]
Single-atom Ag/g-C_3N_4	Cyanamide, potassium tricyanomethanide, $AgNO_3$	Degradation of bisphenol A	[139]
Single-atom Ag/carbon quantum dots/g-C_3N_4	Citric acid, sodium tricyanomethanide, $AgNO_3$	Photocatalytic degradation of naproxen	[17]
Single-atom Ag/g-C_3N_4	$AgNO_3$, sodium tricyanomethanide,	Photocatalytic degradation of sulfamethazine	[141]
Ultrafine silver nanoparticles/g-C_3N_4	Melamine, $AgNO_3$	Photocatalytic degradation of rhodamine B and tetracycline hydrochloride	[142]
Single-atom Ag/g-C_3N_4	Melamine, $AgNO_3$	Photocatalytic degradation of naproxen	[140]
Single-atom Ag/g-C_3N_4	Dicyandiamide, $C_5H_7AgO_2$	Photocatalytic hydrogen evolution	[45]
AgX/g-C_3N_4 (X = Br, I)	Dicyandiamide, 1-hexadecyl-3-methylimidazolium bromide, $AgNO_3$	Photocatalytic degradation of methyl orange	[143]
Ag_3PO_4/g-C_3N_4	Melamine, Na_2HPO_4, $AgNO_3$	Photocatalytic degradation of rhodamine B	[144]
Ag_2O/g-C_3N_4	Melamine, $AgNO_3$	Photocatalytic degradation of rhodamine B	[145]
AgBr/g-C_3N_4	Melamine, CTAB, $AgNO_3$	Photocatalytic degradation of methyl orange	[146]
Ag_2CO_3/g-C_3N_4	Melamine, $NaHCO_3$, $AgNO_3$	Photocatalytic degradation of methyl orange and rhodamine B	[147]
Ag_3PO_4/g-C_3N_4	cyanuric acid, melamine, $AgNO_3$, Na_3PO_4	Photocatalytic water oxidation	[155]
Ag_2CrO_4/g-C_3N_4	$AgNO_3$, K_2CrO_4, guanidine hydrochloride,	Photocatalytic degradation of rhodamine B and phenol	[148]
Ag_2NCN/g-C_3N_4	Melamine, $AgNO_3$, cyanamide	Photocatalytic hydrogen evolution	[157]
Ag_2NCN/g-C_3N_4	Urea, $AgNO_3$, cyanamide	Photocatalytic degradation of methyl orange and methylene blue	[149]
Ag_2CrO_4/g-C_3N_4/graphene oxide	Urea, graphite powers, K_2CrO_4, $AgNO_3$	Photocatalytic CO_2 reduction	[158]
Ag-$AgVO_3$/g-C_3N_4	$AgNO_3$, NH_4VO_3	Photocatalytic degradation of tetracycline	[150]
AgCl/g-C_3N_4	Melamine, $AgNO_3$, NaCl	Photocatalytic degradation of tetracycline	[151]
AgBr/P-g-C_3N_4	Urea, melamine, $AgNO_3$, NaBr	Photocatalytic degradation of ephedrine	[152]
Ag/AgBr/g-C_3N_4/graphene oxide	Melamine, $AgNO_3$, KBr	Photocatalytic hydrogen evolution	[156]
AgI/g-C_3N_4	Melamine, $LiI{\cdot}2H_2O$, $AgNO_3$	Photocatalytic degradation of rhodamine B and methyl orange	[153]
Ag@AgCl/g-C_3N_4	Melamine, $AgNO_3$, NaClO	Photocatalytic degradation of tetracycline	[154]

nitride *via in-situ* decomposition-thermal polymerization method. The obtained Ag/B-doped g-C_3N_4 composites were used for photocatalytic ammonia production and the photocatalytic property was distinguished due to inhibiting the recombination of photogenerated charge carriers by the loaded Ag nanoparticles [133]. The applications of g-C_3N_4 decorated with Ag nanoparticles had been further extended for sensing. Cheng *et al.* synthesized a composite of g-C_3N_4 quantum dots decorated with Ag nanoparticles, which had strong metal-enhanced fluorescence intensity and was used for ultrasensitive detection of heparin [75]. The parathion-methyl [134] and Hg^{2+} ion [135] were also detected using Ag nanoparticles decorated g-C_3N_4 as sensor. Interestingly enough, Bayan *et al.* fabricated a textile based triboelectric nanogenerator for the first time, which was made up of Ag nanoparticles loaded

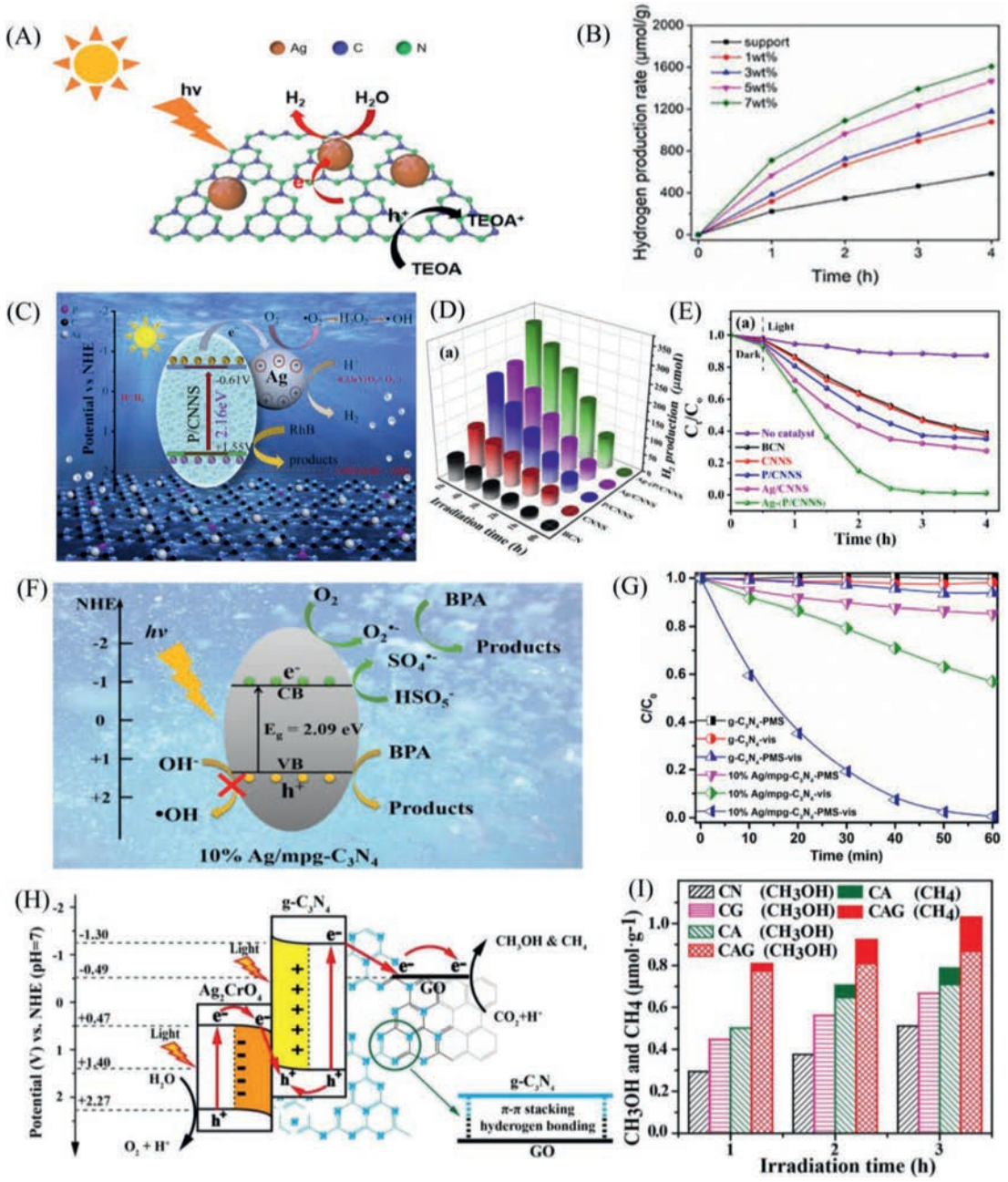

Fig. 6. Schematic diagram (A) and H_2 generation rate of catalysts with different loading contents (B) of photocatalytic hydrogen generation of Ag/g-C_3N_4. Reprinted with permission [132]. Copyright 2022, Elsevier. Photocatalytic mechanism of Ag decorated P-doped g-C_3N_4 nanosheets under visible-light irradiation (C), time course of hydrogen evolution (D), and photocatalytic activities (E) for rhodamine B degradation under visible light irradiation. Reprinted with permission [43]. Copyright 2022, Elsevier. The possible photocatalytic mechanism (F) and photocatalytic activity (G) for degradation of bisphenol A over photocatalyst of mesoporous g-C_3N_4 decorated with isolated Ag sites. Reprinted with permission [139]. Copyright 2017, Elsevier. The proposed Z-scheme photocatalytic mechanism for the Ag_2CrO_4/g-C_3N_4/GO composite (H) and CH_3OH and CH_4 production (I) of CN (g-C_3N_4), CG (g-C_3N_4/GO), CA (Ag_2CrO_4/g-C_3N_4) and CAG (Ag_2CrO_4/g-C_3N_4/GO) samples. Reprinted with permission [158]. Copyright 2018, Elsevier.

g-C_3N_4 nanosheets and carbon fibres. The superior output characteristics and thermal stability of triboelectric nanogenerator made it become potential power sources for wearable electronics [42].

3.2. The g-C_3N_4 decorated with silver nanoclusters

During the rational design of silver-modified g-C_3N_4 photocatalysts for hydrogen evolution, researchers paid great attention to adjust the size of silver (Ag) nanoparticles to enhance the photocatalytic property. Recently, Mallikarjuna *et al.* successfully fabricated g-C_3N_4 decorated with Ag nanoclusters using ultrasonication method. The obtained Ag/g-C_3N_4 composite displayed the profound photocatalytic activities for hydrogen evolution. Furthermore, the effect of dye degradation and antimicrobial activity were profound [136]. Chen *et al.* constructed the highly efficient photocatalysts of Ag decorated P-doped g-C_3N_4 for hydrogen evolution and photocatalytic degradation of rhodamine B, which were severally 5.3 and 1.6 times that of bulk g-C_3N_4 due to the plasma resonance effect of Ag and Schottky junction between Ag and P-doped g-C_3N_4 (Figs. 6C-E) [43]. Besides, the various pollutants such as rhodamine B, tetracycline, and acetaminophen could be degraded by Ag/g-C_3N_4 composite, including the g–C_3N_4 nanosheets decorated with silver silicates dots (~5.2 nm) [55] and silver nanoclusters [137,138].

3.3. The g-C_3N_4 decorated with single atom silver

As a representative n-type polymer semiconductor, the g-C_3N_4 had been employed as excellent host support for producing single-atom photocatalysts due to the abundant surface trapping sites for isolated atoms. The noble metal silver (Ag) had been decorated on the g-C_3N_4 to fabricate the single atom-dispersed silver-decorated g-C_3N_4 photocatalysts for the degradation of emerging pollutants and hydrogen evolution. Wang *et al.* had decorated isolated Ag atoms on mesoporous g-C_3N_4 (mpg-C_3N_4) *via* co-condensation method. The as-synthesized Ag/mpg-C_3N_4 single-atom photocatalyst presented excellent performance for the degradation of bisphenol A (100% degradation over 0.1 g/L photocatalysts within 1 h) due to quick transfer of photoexcited electrons by adding peroxymonosulfate to accelerate the separation of electron-hole pairs, as seen from Figs. 6F and G [139]. Wang *et al.* reported a novel ternary photocatalyst comprised of single atom-dispersed Ag and carbon quantum dots, co-loaded with ultrathin g-C_3N_4, which presented a highly photocatalytic activity for the degradation of naproxen, mainly attributing to the surface plasmon resonance effect and the electron separation and transfer capacity of Ag [17]. Recently, Zhao *et al.* have further demonstrated that Ag/g-C_3N_4 single-atom photocatalyst showed the enhanced visible light absorption and accelerated charge transfer owing to the amorphous structure induced by single-atom Ag, thus giving much better photocatalytic naproxen degradation activity than the pure g-C_3N_4 [140]. Besides, Wang *et al.* also synthesized a single-atom dispersed Ag loaded ultrathin g-C_3N_4 hybrid by a facile co-polymerization, which was served as visible light driven photocatalyst for the degradation of sulfamethazine and exhibited higher efficiency [141]. Soon afterwards, Wang *et al.* synthesized the sodium ion-doped g-C_3N_4 photocatalyst decorated with ultrafine silver nanoparticles (<1 nm) *via* facile and efficient one-pot route, which showed enhanced photogenerated charge separation/transfer and effectively degraded rhodamine B and tetracycline hydrochloride [142]. Artificial photocatalytic hydrogen evolution was a potential path to convert the infinite and freely accessible solar energy into the green and clean energy carrier of hydrogen. Lately, Li *et al.* constructed the highly active photocatalyst of single-atom silver-decorated g-C_3N_4, which showed excellent activity for the photocatalytic hydrogen evolution [45].

3.4. The g-C_3N_4 decorated with other kinds of silver

Other kinds of silvers, including silver halides, Ag_3PO_4, Ag_2O, Ag_2CO_3, Ag_2CrO_4, Ag_2NCN, Ag/AgO, Ag-$AgVO_3$, Ag@AgCl, had also been applied to construct g-C_3N_4-based photocatalysts. Organic pollutants such as dyes, pharmaceuticals had undesirable hazards on human settlements and ecological balance. It was urgent to efficiently eliminate the contaminants and achieve a sustainable planet. Photocatalytic degradation provided an interesting approach to remove these contaminants by rational design of photocatalysts and harvesting solar energy to promote the generation of free radical species. Xu *et al.* had decorated the AgX (X = Br, I) nanoparticles onto the g-C_3N_4 for the photocatalytic degradation of methyl orange [143]. The introduction of AgX nanoparticles promoted the photocurrent and increased photocatalytic activity. In the same year, Zhang *et al.* developed a novel g-C_3N_4/Ag_3PO_4 bulk heterojunction for photocatalytic degradation of rhodamine B, which had two intense optical absorption edges corresponding to g-C_3N_4 and Ag_3PO_4 in the visible light region [144]. Afterwards, more and more photocatalysts, including Ag_2O-g-C_3N_4 composite [145], AgBr/g-C_3N_4 nanocomposite photocatalyst [146], g-C_3N_4 nanosheets decorated with Ag_2CO_3 nanoparticles [147], g-C_3N_4 sheets decorated with Ag_2CrO_4 nanoparticles [148], ultrathin g-C_3N_4 nanosheets decorated with Ag_2NCN nanoparticles [149], the g–C_3N_4 microspheres decorated with silver/silver(II) oxide (Ag/AgO) [96], Ag-$AgVO_3$/g-C_3N_4 composite [150], poly-*o*-phenylenediamine modified AgCl/g-C_3N_4 nanosheets [151], Z-scheme AgBr/P-g-C_3N_4 heterojunction photocatalyst [152], AgI/g-C_3N_4 nanocomposites [153], and Ag@AgCl/g-C_3N_4 plasmonic photocatalyst [154], had been used for the photocatalytic degradation of rhodamine B [145,147,148,153], methyl orange [146,147,153], phenol [148], organic dye [149], acid violet-7 dye [96], tetracycline [150,151,154], ephedrine [152]. Furthermore, Yang *et al.* reported a highly efficient photocatalyst of decorating silver phosphate particles on various g-C_3N_4 for the photocatalytic hydrogen evolution [155]. The Z-scheme and p-n heterostructure of porous g-C_3N_4/graphene oxide-Ag/AgBr composite was constructed for high-efficient photocatalytic hydrogen evolution (3.69 mmol g^{-1} h^{-1}) at the absence of Pt co-catalyst, which was higher than the largest number of existing photocatalysts [156]. Nevertheless, Bai *et al.* further fabricated heterojunction materials composed of Ag_2NCN and g-C_3N_4 for photocatalytic hydrogen evolution, which exhibited higher photocatalytic activity (322.35 μmol g^{-1} h^{-1}) [157]. In addition, the ternary nanocomposite Z-scheme photocatalyst composed of Ag_2CrO_4, g-C_3N_4 and graphene oxide was fabricated for photocatalytic CO_2 reduction, which exhibited an enhanced CO_2 conversion activity owing to the broadened light absorption, higher CO_2 adsorption and more efficient charge separation, as seen from Figs. 6H and I [158]. As a consequence, the g-C_3N_4-based photocatalysts held great promise on photocatalytic energy conversion.

4. Summary and outlook

In conclusion, we had summarized the several desirable properties of g-C_3N_4 such as tunable electronic band structure, high physical and chemical stability, optical performances, electrochemical and photoelectrochemical performances and the multifarious types, including nanocluster, nanosphere, nanorod, nanotube, nanofiber/nanowire, nanosheet. The g-C_3N_4 nanoclusters had strong quantum confinement effects and thus displayed the bright fluorescence. Besides, the g-C_3N_4 nanosphere, nanorod, nanotube and nanofiber/nanowire were widely used for photocatalysis owing to high surface area, smooth carrier transport and light harvesting. Most important of all, the g-C_3N_4 nanosheets were the most widely used in the photocatalytic field because of graphite-like layered structure and weak van der Waals of interlamination. Furthermore, the photocatalytic reactions of various silver-modified g-C_3N_4 were summarized in detail and comprehensively, especially the g-C_3N_4 decorated with silver nanoparticles, silver nanoclusters and single atom silver for the photocatalytic hydrogen evolution, pollutants degradation and CO_2 reduction. Among them, the single atom silver could provide the 100% utilization of active metal sites due to the presence of isolated silver atoms and thus exhibited more excellent catalytic behavior compared with nanoparticles and nanoclusters. It had no doubt that silver-modified g-C_3N_4 photocatalysts were excellent candidates owing to the accelerated charge separation/transfer efficiency and promoting photocatalytic activities. Apart from the aforementioned excellent achievements, there was still certain challenges in the exploration and actual applications of various silver-modified g-C_3N_4 photocatalysts, including the achievement of long-term stability, the high loading of various silver (especially single atom silver), the practical application scope in the field of energy conversion.

Declaration of competing interest

The authors declare that they have no known competing financial interests or personal relationships that could have appeared to influence the work reported in this paper.

Acknowledgments

This study was financially supported by the Shenzhen Science and Technology Program (No. JCYJ20220531093205013), and the National Natural Science Foundation of China (No. 52100069).

References

[1] D. Li, X. Li, J. Gong, Chem. Rev. 116 (2016) 11529–11653.
[2] Y. Xing, X. Wang, S. Hao, et al., Chin. Chem. Lett. 32 (2021) 13–20.
[3] S. Patnaik, D.P. Sahoo, K. Parida, Carbon 172 (2021) 682–711.
[4] L. Zhang, Z.J. Zhao, T. Wang, J. Gong, Chem. Soc. Rev. 47 (2018) 5423–5443.
[5] Q. Zeng, S. Chang, M. Wang, et al., Chin. Chem. Lett. 32 (2021) 2212–2216.
[6] B.H. Kreps, Am. J. Econ. Sociol. 79 (2020) 695–717.
[7] J.D. Xiao, H.L. Jiang, Acc. Chem. Res. 52 (2019) 356–366.
[8] P. Zhang, X.W. Lou, Adv. Mater. 31 (2019) 1900281.
[9] Z.H. Xue, D. Luan, H. Zhang, X.W. Lou, Joule 6 (2022) 92–133.
[10] J. Liu, H. Wu, F. Li, et al., Adv. Sustain. Syst. 4 (2020) 2000151.
[11] J. Liang, X. Yang, Y. Wang, et al., J. Mater. Chem. A 9 (2021) 12898–12922.
[12] Q. Zhang, Y. Xiao, L. Yang, et al., Chin. Chem. Lett. 34 (2023) 107628.
[13] Z. fiqar, J. Tao, T. Yang, et al., Surf. Interfaces 26 (2021) 101312.
[14] X. Wang, H. Jiang, M. Zhu, X. Shi, Chin. Chem. Lett. 34 (2023) 107683.
[15] G. Xu, H. Zhang, J. Wei, et al., ACS Nano 12 (2018) 5333–5340.
[16] Y. Liu, L. Chen, X. Liu, et al., Chin. Chem. Lett. 33 (2022) 1385–1389.
[17] F. Wang, Y. Wang, Y. Feng, et al., Appl. Catal. B: Environ. 221 (2018) 510–520.
[18] G. Mamba, A.K. Mishra, Appl. Catal. B: Environ. 198 (2016) 347–377.
[19] J. Liu, Y. Liu, N. Liu, et al., Science 347 (2015) 970–974.
[20] S. Patnaik, D.P. Sahoo, K.M. Parida, J. Colloid Interface Sci. 560 (2020) 519–535.
[21] N. Cheng, P. Jiang, Q. Liu, et al., Analyst 139 (2014) 5065–5068.
[22] S. Patnaik, K.K. Das, A. Mohanty, K. Parida, Catal. Today 315 (2018) 52–66.
[23] P. Xia, B. Zhu, J. Yu, S. Cao, M. Jaroniec, J. Mater. Chem. A 5 (2017) 3230–3238.
[24] J. Zhao, L. Ma, H. Wang, et al., Appl. Surf. Sci. 332 (2015) 625–630.
[25] R. Zhang, S. Niu, X. Zhang, et al., Appl. Surf. Sci. 489 (2019) 427–434.
[26] N. Sagara, S. Kamimura, T. Tsubota, T. Ohno, Appl. Catal. B: Environ. 192 (2016) 193–198.
[27] W. Chen, T.Y. Liu, T. Huang, X.H. Liu, X.J. Yang, Nanoscale 8 (2016) 3711–3719.
[28] S.P. Adhikari, Z.D. Hood, VW. Chen, et al., Sustain. Energy Fuels 2 (2018) 2507–2515.
[29] W. Zhao, Y. Li, P. Zhao, et al., Chem. Eng. J. 405 (2021) 126555.
[30] Q. Chen, C. Yuan, C. Zhai, Chin. Chem. Lett. 33 (2022) 983–986.
[31] H. Liu, X. Liu, W. Yang, et al., J. Mater. Chem. A 7 (2019) 2022–2026.
[32] I.F. Teixeira, E.C.M. Barbosa, S.C.E. Tsang, P.H.C. Camargo, Chem. Soc. Rev. 47 (2018) 7783–7817.
[33] Y. Bu, Z. Chen, W. Li, Appl. Catal. B: Environ. 144 (2014) 622–630.
[34] J.M. Luther, P.K. Jain, T. Ewers, A.P. Alivisatos, Nat. Mater. 10 (2011) 361–366.
[35] F. Wu, C. Pu, M. Zhang, B. Liu, J. Yang, Surf. Interfaces 25 (2021) 101298.
[36] Y. Yang, W. Guo, Y. Guo, et al., J. Hazard. Mater. 271 (2014) 150–159.
[37] S. Ren, G. Zhao, Y. Wang, B. Wang, Q. Wang, Nanotechnology 26 (2015) 125403.
[38] A. Jakab, C. Rosman, Y. Khalavka, et al., ACS Nano 5 (2011) 6880–6885.
[39] C. Clavero, Nat. Photonics 8 (2014) 95–103.
[40] K. Huang, C. Li, L. Wang, W. Wang, X. Meng, Chem. Eng. J. 425 (2021) 131493.
[41] J. Wang, J. Cong, H. Xu, et al., ACS Sustain. Chem. Eng. 5 (2017) 10633–10639.
[42] S. Bayan, S. Pal, S.K. Ray, Nano Energy 94 (2022) 106928.
[43] Y. Chen, X. Ren, X. Wang, et al., Int. J. Hydrog. Energy 47 (2022) 250–263.
[44] I. Majeed, U. Manzoor, F.K. Kanodarwala, et al., Catal. Sci. Technol. 8 (2018) 1183–1193.
[45] X. Li, S. Zhao, X. Duan, et al., Appl. Catal. B: Environ. 283 (2021) 119660.
[46] S. Lv, C. Wu, Y.H. Ng, et al., Int. J. Hydrog. Energy 47 (2022) 42136–42149.
[47] A. Mishra, A. Mehta, S. Basu, et al., Carbon 149 (2019) 693–721.
[48] A. Balakrishnan, M. Chinthala, Chemosphere 297 (2022) 134190.
[49] J. Fu, J. Yu, C. Jiang, B. Cheng, Adv. Energy Mater. 8 (2018) 1701503.
[50] S. Cao, J. Low, J. Yu, M. Jaroniec, Adv. Mater. 27 (2015) 2150–2176.
[51] Y. Zheng, L. Lin, B. Wang, X. Wang, Angew. Chem. Int. Ed. 54 (2015) 12868–12884.
[52] T. Xiong, W. Cen, Y. Zhang, F. Dong, ACS Catal. 6 (2016) 2462–2472.
[53] S. Wang, L. Wang, H. Cong, et al., J. Environ. Chem. Eng. 10 (2022) 108189.
[54] P. Ding, H. Ji, P. Li, et al., Appl. Catal. B: Environ. 300 (2022) 120633.
[55] S. Zhang, H. Gao, X. Liu, et al., ACS Appl. Mater. Interfaces 8 (2016) 35138–35149.
[56] Z. Cai, J. Chen, S. Xing, D. Zheng, L. Guo, J. Hazard. Mater. 416 (2021) 126195.
[57] L. Liu, J. Zhang, B. Zhang, et al., Green Chem. 20 (2018) 4206–4209.
[58] Y. Ren, Q. Han, Y. Zhao, H. Wen, Z. Jiang, J. Hazard. Mater. 404 (2021) 124153.
[59] X. Wang, S. Blechert, M. Antonietti, ACS Catal. 2 (2012) 1596–1606.
[60] J. Liu, H. Wang, M. Antonietti, Chem. Soc. Rev. 45 (2016) 2308–2326.
[61] J. He, X. Wang, S. Jin, Z.Q. Liu, M. Zhu, Chin. J. Catal. 43 (2022) 1306–1315.
[62] B.V. Lotsch, M. Döblinger, J. Sehnert, et al., Chem. Eur. J. 13 (2007) 4969–4980.
[63] Z. Gu, Y. Asakura, S. Yin, Nanotechnology 31 (2019) 114001.
[64] D. Das, S.L. Shinde, K.K. Nanda, ACS Appl. Mater. Interfaces 8 (2016) 2181–2186.
[65] Q.X. Luo, Y. Li, R.P. Liang, et al., Electroanal. Chem. 856 (2020) 113706.
[66] X. Wang, K. Maeda, A. Thomas, et al., Nat. Mater. 8 (2009) 76–80.
[67] J.S. Zhang, X.F. Chen, K. Takanabe, et al., Angew. Chem. Int. Ed. 49 (2010) 441–444.
[68] A. Thomas, A. Fischer, F. Goettmann, et al., J. Mater. Chem. 18 (2008) 4893–4908.
[69] Q.M. Feng, Y.Z. Shen, M.X. Li, et al., Anal. Chem. 88 (2016) 937–944.
[70] A. Wang, C. Wang, L. Fu, W. Wong-Ng, Y. Lan, Nano-Micro Lett. 9 (2017) 47.
[71] X. Wang, A. Vasileff, Y. Jiao, Y. Zheng, S.Z. Qiao, Adv. Mater. 31 (2019) 1803625.
[72] Y. Zhang, M. Antonietti, Chem. Asian J. 5 (2010) 1307–1311.
[73] W.J. Ong, L.L. Tan, Y.H. Ng, S.T. Yong, S.P. Chai, Chem. Rev. 116 (2016) 7159–7329.
[74] L. Shi, T. Wang, H. Zhang, K. Chang, J. Ye, Adv. Funct. Mater. 25 (2015) 5360–5367.
[75] Q. Cheng, Y. He, Y. Ge, J. Zhou, G. Song, Microchim. Acta 185 (2018) 332.
[76] T. Alizadeh, F. Rafiei, Mater. Chem. Phys. 227 (2019) 176–183.
[77] S.M. Abdel Moneim, T.A. Gad-Allah, M.F. El-Shahat, A.M. Ashmawy, H.S. Ibrahim, J. Environ. Chem. Eng. 4 (2016) 4165–4172.
[78] X. Deng, X. Kuang, J. Zeng, et al., Nanotechnology 33 (2022) 175401.
[79] K. Wang, Q. Li, B. Liu, et al., Appl. Catal. B: Environ. 176–177 (2015) 44–52.
[80] J. Xiao, Y. Xie, F. Nawaz, et al., Appl. Catal. B: Environ. 183 (2016) 417–425.
[81] X.D. Sun, Y.Y. Li, J. Zhou, et al., J. Colloid Interf. Sci. 451 (2015) 108–116.
[82] G. Liu, T. Wang, H. Zhang, et al., Angew. Chem. 127 (2015) 13765–13769.
[83] Y. Shiraishi, Y. Kofuji, H. Sakamoto, et al., ACS Catal. 5 (2015) 3058–3066.
[84] Z. Tong, D. Yang, Z. Li, et al., ACS Nano 11 (2017) 1103–1112.
[85] J. Xu, H.T. Wu, X. Wang, et al., Phys. Chem. Chem. Phys. 15 (2013) 4510–4517.
[86] L. Shi, L. Liang, F. Wang, J. Ma, J. Sun, Catal. Sci. Technol. 4 (2014) 3235–3243.
[87] F. Dong, L. Wu, Y. Sun, et al., J. Mater. Chem. 21 (2011) 15171–15174.
[88] J.P. Mathias, E.E. Simanek, J.A. Zerkowski, C.T. Seto, G.M. Whitesides, J. Am. Chem. Soc. 116 (1994) 4316–4325.
[89] W. Wang, J.C. Yu, Z. Shen, D.K.L. Chan, T. Gu, Chem. Commun. 50 (2014) 10148–10150.
[90] X. Zhang, H. Wang, H. Wang, et al., Adv. Mater. 26 (2014) 4438–4443.
[91] S. Zhang, J. Li, M. Zeng, et al., Nanoscale 6 (2014) 4157–4162.
[92] X. Cao, J. Ma, Y. Lin, et al., Spectrochim. Acta A 151 (2015) 875–880.
[93] Y.C. Lu, J. Chen, A.J. Wang, et al., J. Mater. Chem. C 3 (2015) 73–78.
[94] J. Wu, S. Yang, J. Li, et al., Adv. Optical Mater. 4 (2016) 2095–2101.
[95] R. Cui, C. Liu, J. Shen, et al., Adv. Funct. Mater. 18 (2008) 2197–2204.
[96] D. Vidyasagar, S.G. Ghugal, A. Kulkarni, et al., Appl. Catal. B: Environ. 221 (2018) 339–348.
[97] J. Ruan, X. Wu, Y. Wang, et al., J. Mater. Chem. A 7 (2019) 19305–19315.
[98] J. Liu, J. Huang, H. Zhou, M. Antonietti, ACS Appl. Mater. Interfaces 6 (2014) 8434–8440.
[99] X.H. Li, X. Wang, M. Antonietti, Chem. Sci. 3 (2012) 2170–2174.
[100] Y. Zheng, L. Lin, X. Ye, F. Guo, X. Wang, Angew. Chem. Int. Ed. 53 (2014) 11926–11930.
[101] Q. Guo, Y. Xie, X. Wang, et al., Chem. Commun. 4 (2004) 26–27.
[102] J. Li, C. Cao, H. Zhu, Nanotechnology 18 (2007) 115605.
[103] S.W. Bian, Z. Ma, W.G. Song, J. Phys. Chem. C 113 (2009) 8668–8672.
[104] S. Wang, C. Li, T. Wang, et al., J. Mater. Chem. A 2 (2014) 2885–2890.
[105] F. He, G. Chen, J. Miao, et al., ACS Energy Lett. 1 (2016) 969–975.
[106] Z. Tong, D. Yang, Y. Sun, Y. Nan, Z. Jiang, Small 12 (2016) 4093–4101.
[107] Y. Zhao, Z. Liu, W. Chu, et al., Adv. Mater. 20 (2008) 1777–1781.
[108] J. Liu, J. Huang, D. Dontosova, M. Antonietti, RSC Adv. 3 (2013) 22988–22993.
[109] M. Tahir, C. Cao, N. Mahmood, et al., ACS Appl. Mater. Interfaces 6 (2014) 1258–1265.
[110] Y. Hou, Z. Wen, S. Cui, X. Feng, J. Chen, Nano Lett. 16 (2016) 2268–2277.
[111] X. Yuan, C. Zhou, Y. Jin, et al., J. Colloid Interface Sci. 468 (2016) 211–219.
[112] Q. Han, F. Zhao, C. Hu, et al., Nano Res. 8 (2015) 1718–1728.
[113] P. Niu, L. Zhang, G. Liu, H.M. Cheng, Adv. Funct. Mater. 22 (2012) 4763–4770.
[114] S. Yang, Y. Gong, J. Zhang, et al., Adv. Mater. 25 (2013) 2452–2456.
[115] X. Zhang, X. Xie, H. Wang, et al., J. Am. Chem. Soc. 135 (2013) 18–21.
[116] T.Y. Ma, Y. Tang, S. Dai, S.Z. Qiao, Small 10 (2014) 2382–2389.
[117] K. Schwinghammer, M.B. Mesch, V. Duppel, et al., J. Am. Chem. Soc. 136 (2014) 1730–1733.
[118] L. Chen, Z. Song, X. Liu, et al., Analyst 143 (2018) 1609–1614.
[119] S. Yang, X. Feng, X. Wang, K. Müllen, Angew. Chem. Int. Ed. 50 (2011) 5339–5343.
[120] J. Zhang, J. Sun, K. Maeda, et al., Energy Environ. Sci. 4 (2011) 675–678.
[121] O. Fontelles-Carceller, M.J. Muñoz-Batista, M. Fernández-García, A. Kubacka, ACS Appl. Mater. Interfaces 8 (2016) 2617–2627.
[122] Y. Song, J. Qi, J. Tian, S. Gao, F. Cui, Chem. Eng. J. 341 (2018) 547–555.
[123] M.J. Muñoz-Batista, O. Fontelles-Carceller, M. Ferrer, M. Fernández-García, A. Kubacka, Appl. Catal. B: Environ. 183 (2016) 86–95.
[124] S. Gao, H. Ji, P. Yang, et al., Small 19 (2023) 2206114.
[125] L. Ge, C. Han, J. Liu, Y. Li, Appl. Catal. A: Gen. 409-410 (2011) 215–222.
[126] Y. Yang, Y. Guo, F. Liu, et al., Appl. Catal. B: Environ. 142-143 (2013) 828–837.
[127] T. Sano, K. Koike, T. Hori, et al., Appl. Catal. B: Environ. 198 (2016) 133–141.
[128] K.Z. Qi, Y. Li, Y.b. Xie, et al., Front. Chem. 7 (2019) 91.
[129] M.E. Khan, T.H. Han, M.M. Khan, M.R. Karim, M.H. Cho, ACS Appl. Nano Mater. 1 (2018) 2912–2922.
[130] T. Ishaq, M. Yousaf, I.A Bhatti, et al., Int. J. Hydrog. Energy 45 (2020) 31574–31584.
[131] T. Ren, Y. Dang, Y. Xiao, et al., Inorg. Chem. Commun. 123 (2021) 108367.
[132] H. Zhu, K.J. Wu, C.H. He, Chem. Eng. J. 429 (2022) 132412.
[133] X. Yao, W. Zhang, J. Huang, et al., Appli. Catal. A: Gen. 601 (2020) 117647.
[134] Y. Li, M. Wan, G. Yan, P. Qiu, X. Wang, J. Pharm. Anal. 11 (2021) 183–190.
[135] E. Murugan, S. Santhoshkumar, S. Govindaraju, M. Palanichamy, Spectrochim. Acta A 246 (2021) 119036.

[136] K. Mallikarjuna, S.V.P. Vattikuti, R. Manne, et al., Nanomaterials 11 (2021) 2918.
[137] T.M.O. Le, T.H. Lam, T.N. Pham, et al., Polymers 10 (2018) 633.
[138] Y. Ling, G. Liao, P. Xu, L. Li, Sep. Purif. Technol. 216 (2019) 1–8.
[139] Y. Wang, X. Zhao, D. Cao, Y. Wang, Y. Zhu, Appl. Catal. B: Environ. 211 (2017) 79–88.
[140] Z. Zhao, W. Zhang, W. Liu, et al., Sci. Total Environ. 742 (2020) 140642.
[141] F. Wang, Y. Wang, Y. Li, et al., Dalton Trans. 47 (2018) 6924–6933.
[142] K.L. Wang, Y. Li, T. Sun, et al., Appl. Surf. Sci. 476 (2019) 741–748.
[143] H. Xu, J. Yan, Y. Xu, et al., Appl. Catal. B: Environ. 129 (2013) 182–193.
[144] F.J. Zhang, F.Z. Xie, S.F. Zhu, et al., Chem. Eng. J. 228 (2013) 435–441.
[145] L. Shi, L. Liang, J. Ma, F. Wang, J. Sun, Catal. Sci. Technol. 4 (2014) 758–765.
[146] Y. Feng, J. Shen, Q. Cai, H. Yang, Q. Shen, New J. Chem. 39 (2015) 1132–1138.
[147] Y. Li, L. Fang, R. Jin, et al., Nanoscale 7 (2015) 758–764.
[148] L. Shi, L. Liang, F. Wang, M. Liu, J. Sun, Dalton Trans. 45 (2016) 5815–5824.
[149] B. Jia, W. Zhao, L. Fan, et al., Catal. Sci. Technol. 8 (2018) 1447–1453.
[150] D. Chen, B. Li, Q. Pu, et al., J. Hazard. Mater. 373 (2019) 303–312.
[151] L. Sun, C. Liu, J. Li, et al., Chin. J. Catal. 40 (2019) 80–94.
[152] M. Chen, C. Guo, S. Hou, et al., Appl. Catal. B: Environ. 266 (2020) 118614.
[153] Y. Orooji, M. Ghanbari, O. Amiri, M. Salavati-Niasari, J. Hazard. Mater. 389 (2020) 122079.
[154] D. Sun, Y. Zhang, Y. Liu, et al., Chem. Eng. J. 384 (2020) 123259.
[155] X. Yang, Z. Chen, J. Xu, et al., ACS Appl. Mater. Interfaces 7 (2015) 15285–15293.
[156] W. Li, X. Wang, M. Li, et al., Appl. Catal. B: Environ. 268 (2020) 118384.
[157] C. Bai, J. Bi, J. Wu, Y. Han, X. Zhang, New J. Chem. 42 (2018) 16005–16012.
[158] D. Xu, B. Cheng, W. Wang, C. Jiang, J. Yu, Appl. Catal. B: Environ. 231 (2018) 368–380.